



Power Engineering Method for Fuel Cell: An overview

R. Ramesh^{1*}, Selvakumar Periyasamy², Chandu V.V. Muralee Gopi³, Poonam Singh⁴, Tarun Gupta⁵

^{1,2}Department of Chemical Engineering, School of Mechanical, Chemical and Materials Engineering, Adama Science and Technology University, Adama-1888, Ethiopia

³Department of Electrical Engineering, University of Sharjah, P.O. Box 27272, United Arab Emirates

⁴Applied Science Department, IAMR Group of Institution Ghaziabad-India

⁵Department of Architecture College of Engineering and Technology, Wollega University, P.O. Box No. 395, Nekemte, Ethiopia

Abstract

In the study, fuel cell modelling and control schemes are investigated in relation to their utilisation. They discuss the uses of fuel cells in automobiles, utility power systems, and standalone systems that combine wind, solar, and fuel cell technology. Industries are actively focusing on fuel cell design and engineering to improve performance, durability, cost effectiveness, and cold-start capabilities. As a result of this new focus, there is an urgent need for the identification, comprehension, prediction, control, and optimization of numerous transport and electrochemical processes that occur in fuel cells on various length scales. Discussing the design and execution of a fuel cell-based power generation system is the main goal of the study. In light of this, a methodology for developing and putting into practise an effective high power converter system is described. The PEM fuel cell electrical equivalent model, which was tested using the commercial MARK 1020 system, is also included in the study.

The series-resonant converter topology, whose foundation is based on soft-switching approach, is chosen after analysis of the converter topologies that are most appropriate for this application type and satisfying a number of criteria. The converter was created with low component stresses, high frequency operation, and soft-switching commutation in mind. It comprises of an input filter, a full-bridge inverter, a series resonant circuit, and a diode rectifier on the primary side and an output filter on the secondary side. The operational limitations of the system MARK 1020 were taken into consideration when designing the converter.

Keywords: Fuel Cell, Power Engineering,

1. Introduction

Due to its great energy efficiency, minimal environmental impact, and low noise levels, fuel cells are widely acknowledged as the energy-conversion technology for portable, fixed, and mobile power in the twenty-first century. Due to the depletion of fossil fuel supplies and environmental contamination, there has been a rise in interest in the usage of renewable energy sources. Because they are ecologically benign, highly efficient, and renewable cycles, study into the new energy sources, such as solar, wind, and fuel cells, can be used to improve the safety, dependability, and sustainability of the world.

Since they generate electricity from hydrogen using an electrochemical process that almost entirely eliminates noise and pollution and leaves only water and heat as waste products, fuel cells in particular stand out as a suitable energy source in this context. Additionally, they offer a number of benefits such being silent, having a high potential for cogeneration applications, and being flexible for a variety of power and application needs. The study, design, and implementation of fuel cell-based power generation systems is the primary objective of this research, This demands that both the fuel cell model and the power electronic converter be carefully chosen.

In this context, fuel cells in particular stand out as a desirable power source since they produce electricity from hydrogen using an electrochemical process that produces almost no noise or pollutants and only water and heat as waste products. Additionally, they offer a number of benefits such being silent, having a high potential for cogeneration applications, and being flexible for a variety of power and application needs. The study, design, and implementation of fuel cell-based power generation systems is the primary objective of this research, which necessitates the careful selection of both the fuel cell model and the power electronic converter.

The converter's resonant structure, which also provides low component stresses, high frequency operation, soft-switching commutation, and low component stresses, allows it to function under a variety of input and output situations. The voltage controller is in charge of maintaining the converter's output voltage constant under variations in load, and the PEM controller is in charge of enhancing performance by maintaining the PEM fuel cell at its optimum operating point. These two components make up the control of the converter.

The PEM fuel cell findings are provided first, followed by those for the entire system with load disturbance. The findings show that the suggested converter is a wise choice for increasing PEM fuel cell efficiency because it enables proper fuel cell power management while maintaining load requirements and reducing losses through the use of soft-switching control.

Objectives

1. The main objective of the study to discuss about most relevant renewable energy.
2. What is fuel cell and how it may change the future of energy generation?
3. Schematic idea about Hybrid types of energy generation with the help of fuel cell,
4. Market value of fuel cell energy
5. Modern methodology adopted and implemented for the generation of renewable energy.
6. Schematic diagrams for converters required and illustrated methodology adopted.

2. Methodology applied

PEMFCs: Proton Exchange Membrane Fuel Cells: The foundation of proton exchange membrane fuel cells (PEMFCs) is an aqueous electrolyte, or polymer, which transports hydrogen ions because it has liquid water on it. As seen in Figure 1, the PEMFC's primary components are as follows. A PEM fuel cell, which is a static device, directly, isothermally, and continuously converts chemical energy from a fuel into electrical energy. Only the hydrogen and oxygen reaction takes place in this procedure. Only heat and water are produced as by products.

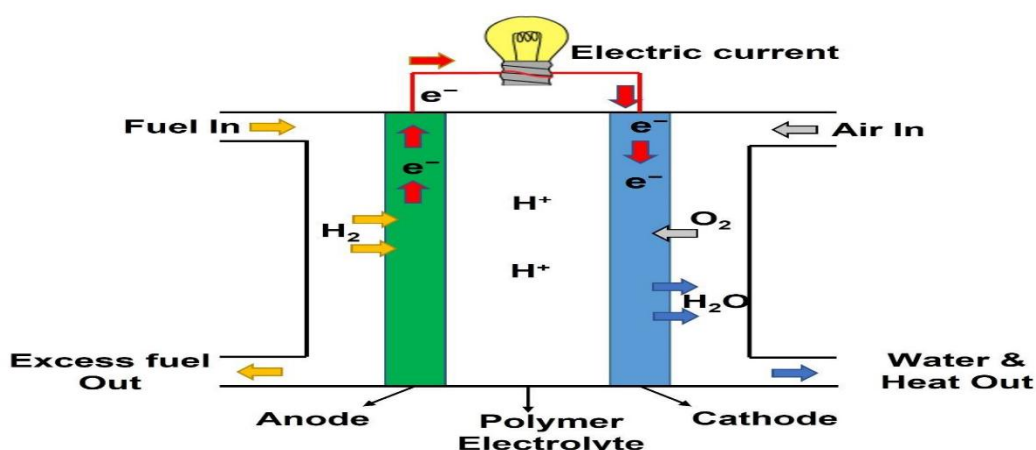
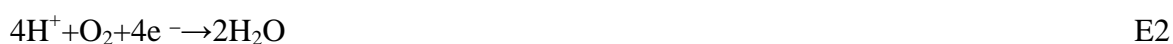


Figure 1. Basic schematic diagram of a PEMFC [32].

A fuel cell is made up of an electrolyte, two electrodes (the anode and cathode), and similar components to a battery. The capacity of a storage battery is limited since it includes all the

components of the electrochemical oxidation-reduction results involved, whereas a fuel cell receives its reactants externally and can run constantly as long as fuel is available. Figure 1 depicts the basic structure of a single cell, while equations 1 to 3 define the reactions occurring on the anode side, cathode side, and throughout the process as a whole. The study's methodology, which is described in detail in Mubarak, 2021.



The overall reaction of the fuel cell is, therefore.



2.1. An analysis of PEM fuel cell modelling

An FC was used in this study to create the experimental inputs and outputs such that they were suitable for the real-time model. Among the components of this circuit design were a converter, a battery charger, and a DC load. These elements made it easier to gauge the FC's production. Figure 2 depicts the corresponding fuel cell simulation. There have been numerous studies and presentations of proton exchange membrane (PEM) fuel cell models in the literature [1–12]. What aspects must be considered in the fuel cell model must be made clear during the selection process [7]. Every application and user has a different model selection process, thus the early choices are crucial to prevent modifications later in the model review process. Theoretical models are typically intricate, difficult, and time-consuming to compute [8,9,11–12]. Without going into great detail about the physical and electrochemical events involved in the operation, the semi-empirical models [1,5,6,10] provide a broad voltage-current connection. These models are frequently distinguished by straightforward implementation and quicker simulation.

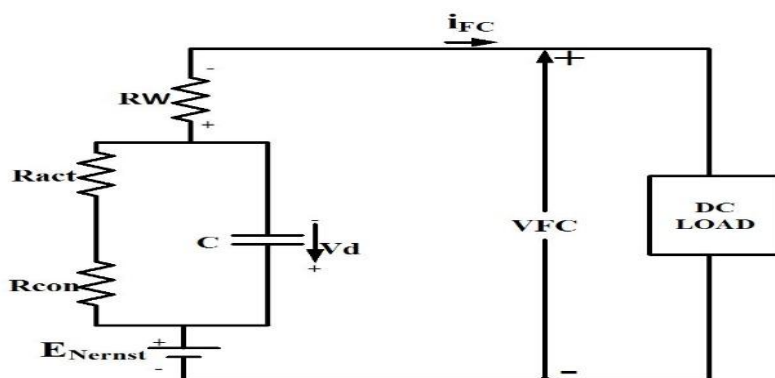


Figure 2: Schematic diagram of Electrical equivalent circuit of the PEM fuel cell [33].

The semi-empirical model used for this investigation corresponds to the electrical equivalent circuit shown in Figure 2. The PEM fuel cell's static and dynamic behaviour are electrically represented by this circuit, which also takes into account the losses and the fuel cell's thermodynamic potential. Equations 4 through 9 describe the PEM's static behaviour, whereas equations 10 and 11 describe its dynamic behaviour. The interface electrode/electrolyte serves as an energy storage element in the capacitor C, which reflects the "charge double layer" fuel cell phenomena. Equations 12 and 13 respectively indicate electrical power and efficiency.

Output voltage of one cell PEMFC cell is defined as:

$$V_{FC} = E_{Nernst} - V_{act} - V_{con} - V_{ohmic} \quad E4$$

Thermodynamic potential:

$$E_{Nernst} = 1.229 + [4.31 * 10^{-5} * T * (\ln PH_2 + 0.5 PO_2)] - [0.85 * 10^{-3} * (T - 298.15)]$$

E5

where T is the fuel cell's temperature in Kelvin (K), P (H₂) is the hydrogen gas partial pressure in atmospheres, and P (O₂) is the oxygen gas partial pressure (atm). Calculations must be made to determine the partial pressure's effectiveness on each surface. The calculation seeks to determine.

Activation over-potential:

The voltage drop resulting from the activation process V_{act} around the anode and cathode electrodes can be mathematically calculated according to the following expression:

$$V_{act} = - [\zeta_1 + \zeta_2 * T + \zeta_3 * \ln(cO_2) * T + \zeta_4 * \ln(I_{FC}) * T] \quad E6$$

Ohmic over-potential:

Ohmic voltage is the voltage that is lost due to resistance when the protons move. The following is the ohmic voltage equation.

$$V_{ohmic} = I_{FC} (RC + RM) \quad E7$$

Concentration over-potential:

Stress related to a loss in concentration is brought on by a shift in concentration level.

$$V_{con} = - B * \ln(1 - J/J_{max}) \quad E8$$

Where: J = actual current density, B = constant (V), and V_{Con} = voltage drop concentration (V) of fuel cell (A/cm²), J_{max} = maximum current density of fuel cell (A/cm²).

voltage produced by the stack:

$$V_s = n * V_{FC} \quad E9$$

The voltage across the capacitor

$$dVd / dt = (1/ C * I_{FC}) - (1/\tau * Vd) \tag{E10}$$

Electrical Time-constant:

$$\tau = C * \{ (V_{act} + V_{con}) / I_{FC} \} \tag{E11}$$

Electrical power:

$$P_{FC} = I_{FC} * V_{FC} \tag{E12}$$

Efficiency:

$$\eta = \mu f * V_{FC} / 1,48 * 100\% \tag{E13}$$

2.2. Experiments conducted using the PEM Mark 1020

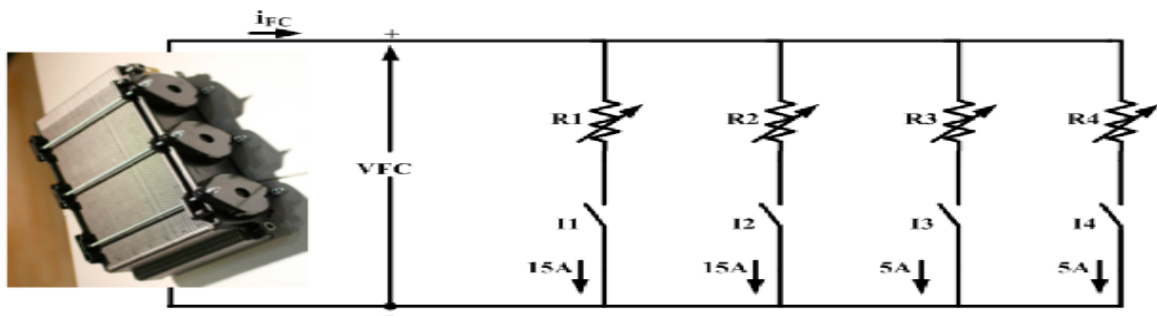


Figure 3. Electrical circuit to assess the Mark 1020 PEM fuel cell [31].

The experimental set-up used to get the electrical PEM properties corresponds to the circuit of Figure 3. Data is logged for each load step to show when the fuel cell reached steady-state performance.

2.2.1. Output voltage and power of PEM Mark 1020

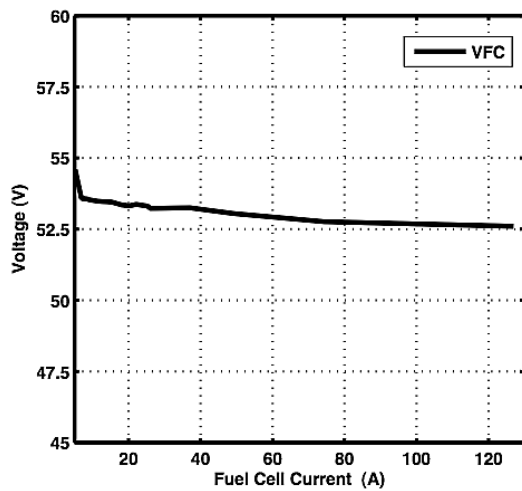


Figure 4. Fuel cell voltage of PEM Mark 1020,

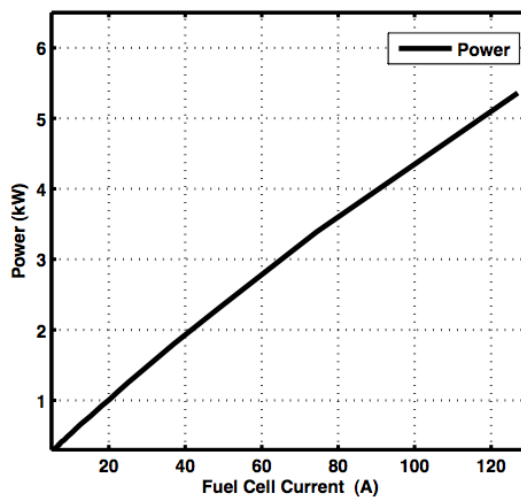


Figure 5. Electrical power [31].

The digital multi-meter is directly connected in parallel with the fuel cell to measure the output voltage. This is an uncontrolled DC voltage that varies depending on the load as well as the amount of fuel the system is receiving. The PEM Mark 1020's stack voltage is depicted in Figure 4 while the stack power is represented in Figure 5. The results for the two electrical variables line up with the information provided by the stack's creator.

2.2.2. The PEM Mark 1020's efficiency and hydrogen consumption

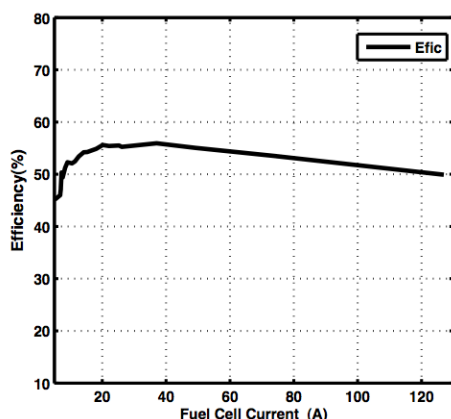


Figure 6. Efficiency of the PEM Mark 1020 [31].

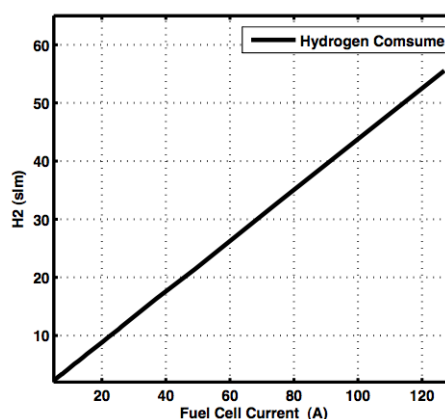


Figure 7. Hydrogen consumed [31].

The lowest and maximum efficiency values for PEM Mark 1020 are 45.16% and 55.47%, respectively. The efficiency range for this product is 49.9% to 55.1%. According to Figure 6, as the current density increases, the efficiency somewhat declines. Figure 7 below shows how the hydrogen used by the stack Mark 1020 is proportionate to the power the fuel cell produces.

2.2.3. Constraints imposed to the converter.

No matter which converter topology is used, the PEM fuel cell's limitations, which include the PEM Mark 1020's minimum and maximum values for voltage, current, and power must be adhered to these values are stated in Table 1 below.

Table 1. Constraints imposed to the power system by PEM MARK 1020.

Ifc (A)	Vfc (V)	Power (W)
2.8	23.71	66
24	19.11	492

3. Power electronic converters for PEM fuel cells

Fuel cell systems employ power electronic converters to transform the DC electrical power through the use of power electronic circuits, fuel cell energy is converted into useful AC or DC power. Numerous solutions have already been described in the literature [14–30] for the power electronic converter, which is a crucial component of the fuel cell system's interface as a power generating system. The converter topologies that can be used are DC-DC along with DC-AC, DC-AC connecting the fuel cell directly to the grid, or DC-DC along with AC-AC isolated by a transformer. The fuel cell's output voltage normally ranges from 20 V to 50 V. Based on how they function, the DC-DC power converters can be divided, as shown in Figure 8. Efficiency is what differentiates them the most from one another. Since greater power converters require a higher power transformer, the single switch topology is not the best option for these converters. Therefore, Push-pull, Half-bridge, and Full-bridge converters—another category of DC-DC isolated converters using multiple switches are discovered.

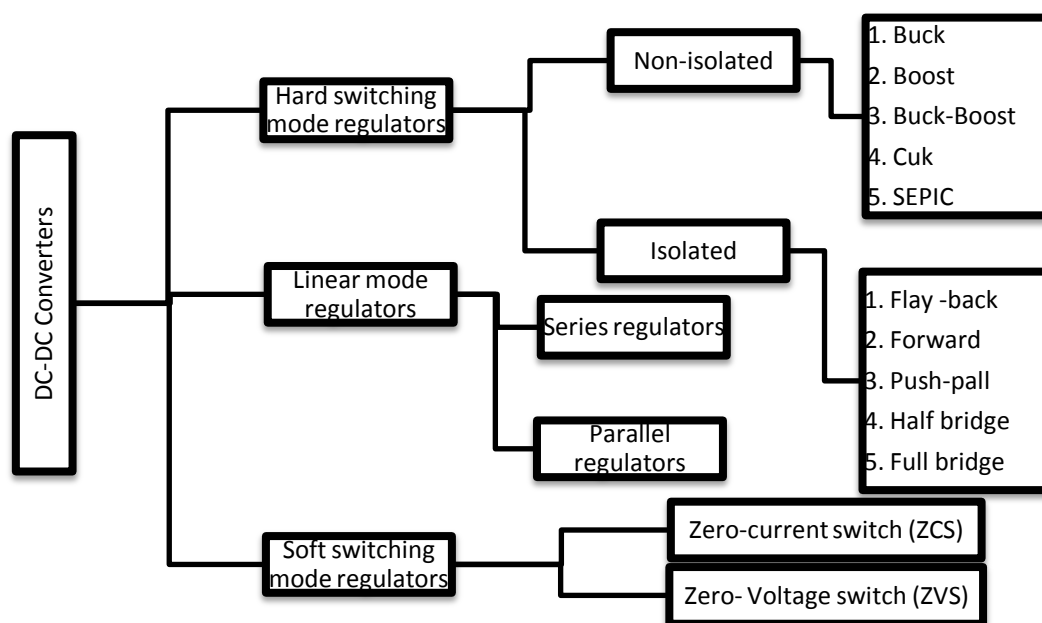


Figure 8. DC-DC power converter classification.

In switched-mode topologies, switching transitions with finite durations would cause significant peak pulse power dissipation in the devices, a loss in converter efficiency, and possibly even transistor breakage during the turn-off transition. Use of load-line snubbers can lessen this issue. The stress on the switches is reduced when snubbers are used. However, the emergence of novel power electronic converters based on soft-switching technologies [15,17,19,20-22,30] has made it possible to raise the switching frequency due to the decline in switching losses and ongoing development of power switches. When the switch voltage or

switch current is zero in this type of converter, the converter switches turn on and turn off [23].

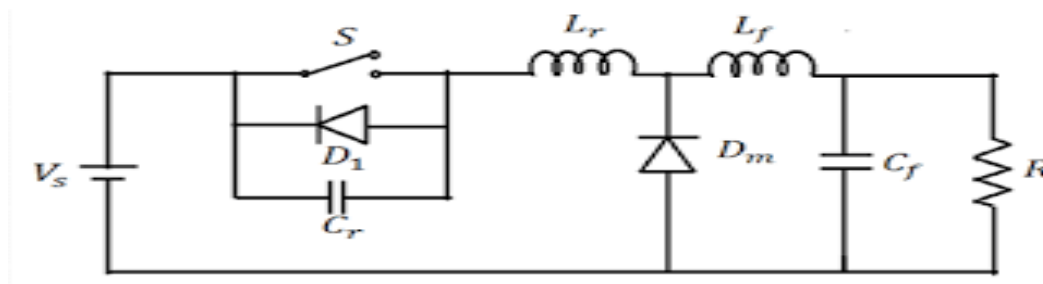


Figure 9. General structure of a resonant converter, ZVS [35,36].

An setup for a soft-switching resonant converter is shown in Figure 9. To aid the switch action, an inductor (L_s) and a capacitor (C_s) have been added. The diode is enhanced by an equivalent LdCd pair. In each of these soft switching scenarios, the ringing resonant waveform is interrupted by switch action at a zero crossing. This method is frequently referred to as quasi-resonance. The resonance or soft switching strategy can be utilised in DC-DC converters to set up the ZCS or ZVS. Figure 9's resonant component can be rearranged to get the ZVS or ZCS. Switching losses at turn-on and turn-off can both be reduced and eliminated with ZCS topologies. The operation of the converter is no longer affected by the junction capacitance of the output diode if a relatively large capacitor is attached across it during resonance. The capacitive turn-on losses are the main ZCS drawback when Mosfets are employed. As a result, switching loss and noise increase with switching frequency. During turn-on, a sizable rate of change of voltage can be linked to the gate drive circuit through the Miller capacitor. The switches' high current stress and significant conduction loss represent another drawback. The capacitive turn-on loss is eliminated by ZVS. It is appropriate for operating at high frequencies. Switches in single-ended configurations may experience excessive voltage stress that is inversely correlated with load. Variable frequency control can be used to control the ZCS and ZVS resonant converters' output. Whereas the ZVS [24] runs on continual off-time control, the ZCS [20-22] runs on constant on-time control.

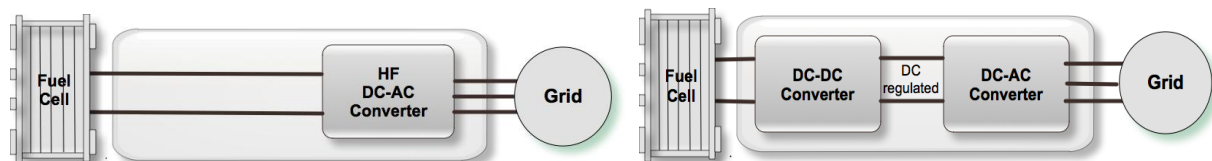
3.1 Requirements for selecting the converter topology.

To ensure the highest efficiency and lowest cost of the power generation system, the following criteria are taken into account when choosing the converter topology. Controlling output voltage in accordance with a reference, Provide current with minimal ripple and

harmonic interference, have high efficiency across the whole operating range, operate correctly under all circumstances, and have built-in filtering and storage options.

3.2. DC-DC converter topologies

The effectiveness and efficiency of the energy generation process based on fuel cells is greatly influenced by power electronic converters in general and DC-DC converters in particular. Static power converters that can accurately support the control methods are necessary for the control of the fuel cell's operating point. When employing converters with fuel cells, the major goal is to maximise efficiency while using the best control methods possible while taking into account the above-mentioned parameters. As previously mentioned, several converter topologies can be applied, as shown in figures 10 A and B below. Between the fuel cell and the inverter, a DC-DC converter is typically used to perform two tasks: 1) acts as DC isolation for the inverter; and 2) generates enough voltage for the inverter input to provide the necessary magnitude of the AC voltage. The utility connection will determine whether the inverter is single-phase or three-phase.



A. DC-AC converter interfaced directly to the grid,
grid

B. DC-AC followed by a AC-AC converter interfacing the
grid

Figure 10. Grid Configuration A and B

3.2.1. Converter in series with a capacitive output filter

According to the above-mentioned principles, the converter architecture in Figure 11 is acceptable. This modified series resonant converter (SRC) soft switches HF switches using a (L-C)||L resonant tank. Some key traits of this kind of converter can be summed up as follows:

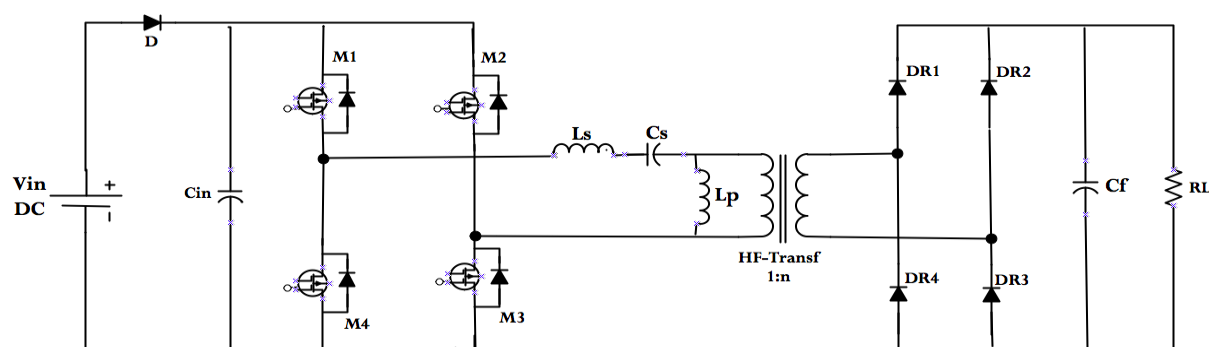


Figure 11. Series Resonant converter with capacitive output filter [31].

High efficiency is provided by this arrangement under all possible load and line circumstances, although it declines when input voltage is raised. It reaches the complete range of ZVS (full load to moderate load). Switch peak current increases dramatically with a change in input voltage but decreases with load.

3.2.2. converter in series with an inductive output filter

The converter topology in Figure 15 is an inductive output filter on an LCL type SRC. This makes use of an LCL resonant tank for the soft switching of high frequency switches and an inductive output filter. These key traits can be summed up as follows. It reaches the complete range of ZVS (full load to moderate load). Although the voltage rating of the rectifier diode is higher, the efficiency is not significantly impacted by the use of ultra-fast recovery diodes with high voltage ratings and minimal forward voltage drops.

This configuration can also be transformed into a series resonant converter (SRC), shown in Figure 12, which uses a (L-C) || C resonant tank for soft switching of high frequency switches. In this situation, the term "series-parallel resonant converter" is also used to describe this arrangement (SPRC).

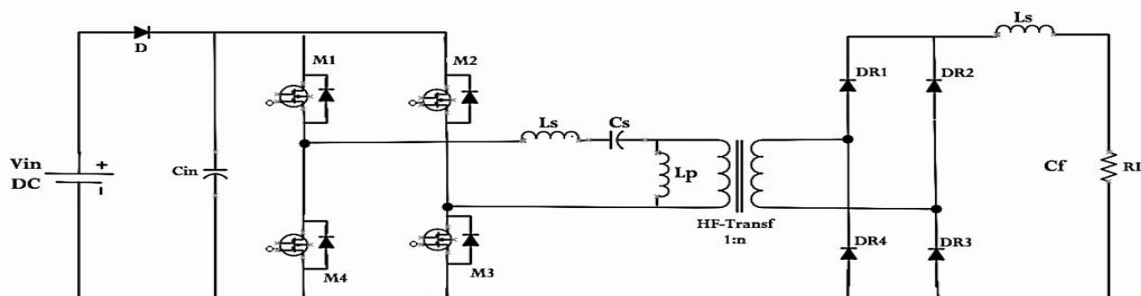


Figure 12. Series Resonant converter with inductive output filter [31].

3.2.3. With an inductive output filter, a PWM full-bridge converter

Figure 13 shows a phase-shifted full bridge converter with an inductive output filter. For high power applications, this soft-switched arrangement is the most popular.

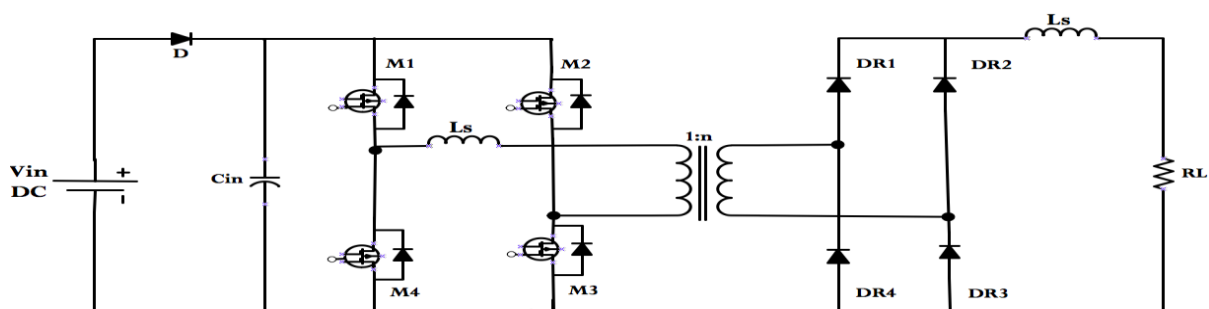


Figure 13. PWM full-bridge converter [31].

This constant frequency converter has a small circulating circuit and ZVS main switches. Filter inductance, transformer leakage inductance, snubber capacitance, and switch junction parasitic capacitances all contribute to the ZVS. The phase shift technique is used to control the output voltage at a consistent frequency. Its primary traits can be summed up as follows: Loss of duty cycle on the secondary side is the main drawback of this design. Rectifier diodes on the secondary side are under high voltage stress. parasitic ringing on the transformer's secondary side. Big inductors may extend ZVS range but necessitate a reduction in transformer turns-ratio (N_p/N_s), which raises main side current and results in significant conduction losses, which reduces converter efficiency. A good compromise between the transformer turns-ratio and leakage inductance is required to maintain low conduction losses..

3.2.4. full-bridge converter with secondary side control

Using a phase-controlled rectifier on the secondary side and a full-bridge inverter on the main side, the arrangement resembles a secondary side controlled converter. With a set duty ratio and complementary gating, the switches on the primary side are actuated. The switches on the secondary side of the HF transformer are adjusted to create a phase mismatch between the voltages on the primary and secondary sides in order to manage the output voltage with load and input line voltage variations. Following is a list of this configuration's primary attributes: Control is easy and simple.

An issue with the converter is that the switches on the secondary side display ZVS or ZCS depending on the line and load. When the input voltage is lower, the secondary side switches display ZVS, and when the input voltage is higher, ZCS. This converter's efficiency, measured at full load and variable line voltage, is close to 92.01%.

3.2.5. two-inductor boost converter that is current-fed.

The voltage-fed half-bridge converter configuration is duplicated in the current-fed two-inductor boost converter. With only two switches utilised on the primary side, this design requires a transformer with an extremely low turns ratio. Since the voltage across the switches is sinusoidal, the primary switches turn off smoothly. The same applies to turning on and off rectifier diodes. At variable line input and load conditions, ZVS is very difficult to achieve due to the large peak and average currents through rectifier diodes. Applications requiring continuous input and output voltage should choose this design.

3.2.6. Bidirectional current-fed converter.

The voltage-fed half-bridge converter configuration is duplicated in the current-fed two-inductor boost converter. With only two switches utilised on the primary side, this design requires a transformer with an extremely low turns ratio. Since the voltage across the switches is sinusoidal, the primary switches turn off smoothly. The same applies to turning on and off rectifier diodes. At variable line input and load conditions, ZVS is very difficult to achieve due to the large peak and average currents through rectifier diodes. Applications requiring continuous input and output voltage should choose this design.

3.3. Selection of converter topology and operation

The chosen topology is a full-bridge series-resonant inverter, a high frequency transformer, and a rectifier, considering the past research. Also, there are two low-pass filters: one on the main side, which shields the PEM from excessive ripple current, and one on the secondary side, which improves the calibre of the energy the power system provides to the load or the grid. Figure 14 below depicts the electrical layout of its topology, also referred to as a series resonant converter (SRC).

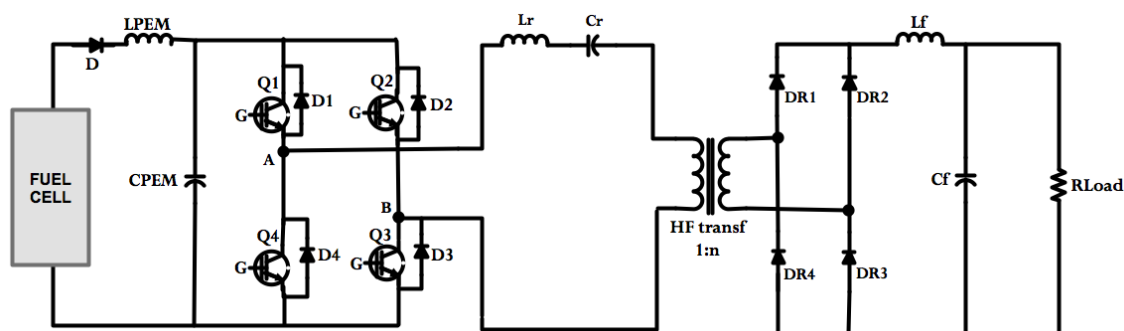


Figure 14. Electrical circuit of the SRC.

The converter operates in the following manner: it must increase the generally low voltage provided by the fuel cell stack to a high and consistent level, such as 48 V or 400 VDC, in order to power an electric vehicle or be delivered to the grid via an inverter. The step-up voltage transformer known as the HF offers galvanic isolation between the high and low voltage levels of the circuits. On the transformer's primary side, the LC series resonant circuit produces sinusoidal voltage and current waveforms. The L_r and C_r components' proper values are chosen, and the circuit's resonance frequency is established. The fuel cell's DC voltage is then rectified on the secondary side of the HF transformer after being initially inverted on the primary side. The low pass filter in the main side (L_{PEM} , C_{PEM}) protects the PEM fuel cell from ripple current and voltage created by the converter and also enables

energy storage in the DC bus. The secondary's low pass filter (L_f , C_f) enables lowering the load's current and voltage ripples, respectively.

3.4. Mathematical analysis of the series resonant converter (SRC)

The series-resonant inverter is made up of a regulated full-bridge and a series resonant circuit with a natural frequency f_r and impedance Z_r as part of the topology of the Electrical Equivalent Circuit (Figure 15) of the SRC.

The tank waveforms, namely the capacitor voltage, V_C , and the inductance current, i_L , are considered to be perfectly sinusoidal in the study of this circuit using the sinusoidal approximation, which ignores the harmonics of the switching frequency.

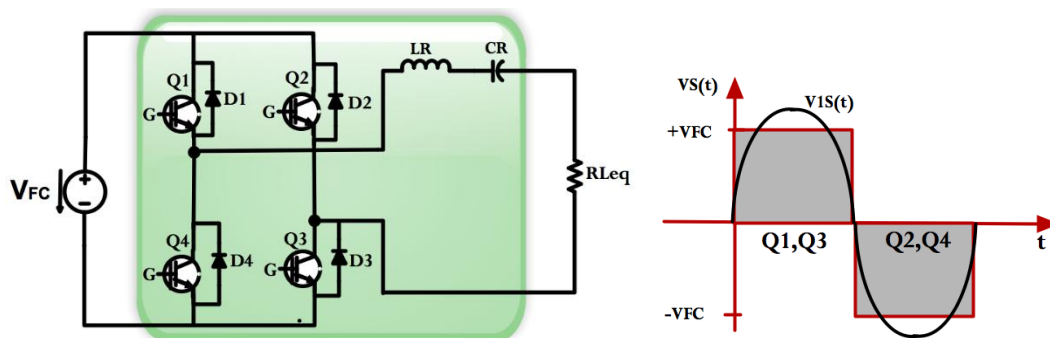


Figure 15. Electrical equivalent circuit of the SRC, Figure 16. Output voltage in a full-bridge inverter.

3.4.1. Voltage

IGBTs Q1 and Q3 conduct in the first half period $[0-\pi]$, while IGBTs Q2 and Q4 conduct in the second half period $[\pi-2\pi]$, as shown in Figure 16. The output voltage of the full-bridge inverter, which is also the input voltage of the series resonant circuit, is a square-waveform in Figure 16.

$$V_{Fc}, \text{ for } 0 < \omega t \leq \pi - V_{Fc}, \text{ for } \pi < \omega t \leq 2\pi \quad \text{E14}$$

3.4.2. Current

In the first half period $[0-\pi]$, the current $i(t)$ equals the output current $+i_s(t)$, and in the second half period $[\pi-2\pi]$, it is its inverse. The tank rings sinusoidal and $i_s(t)$ is well approximated by a sinusoid waveform as shown by equations 15 and 16 under the circumstances mentioned above.

$$i_{Q1} = i_{Q3} = \begin{cases} +I_{max} \times \sin(\omega t - \Phi), & \text{for } 0 < \omega t < \pi \\ -I_{max} \times \sin(\omega t - \Phi), & \text{for } \pi < \omega t < 2\pi \end{cases} \quad \text{E15}$$

$$i_{Q2} = i_{Q4} = \begin{cases} 0, & \text{for } 0 < \omega t < \pi \\ I_{max} \times \sin(\omega t - \Phi), & \text{for } \pi < \omega t < 2\pi \end{cases} \quad \text{E16}$$

The analysis of the SRC can be carried out using a straightforward equivalent circuit, such as that shown in Figure 17, whose operation can be described by the following second-order differential equation.

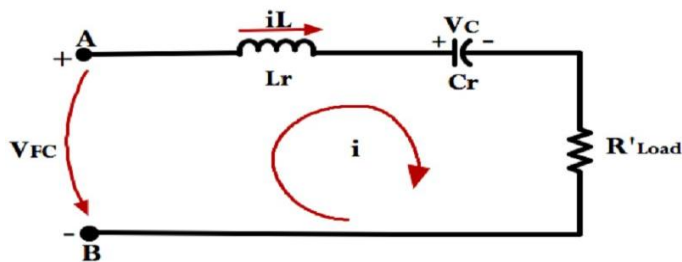


Figure 17. Series resonant circuit with a resistive load.

The Kirchoff loop equation, which states that the sum of voltages around a loop equals zero, is applied to the RLC circuit of Figure 23 to produce the following equation for a series resonant circuit.

$$L_r \frac{di}{dt} + V_{C_r} + RI = V_{FC} \quad \text{E17}$$

Hence equation 18 with $R = Z \cos(\theta)$ expresses the input impedance Z of this circuit. and $X = Z \sin(\theta)$

$$\overline{Z} = R + j(\omega L_r - 1/\omega C_r) \quad \text{E18}$$

3.4.3. Frequency and reactance at an angle

When $X_{L_r} = X_{C_r}$, the reactance of the resonant circuit will become zero, resulting in $Z = R$ and resonant operation, where $f_s = f_r$. Equations 19 and 20 determine this's characteristic impedance Z_r and angular frequency ω_r , respectively.

$$\omega_r = 2\pi f_r = 1/\sqrt{L_r C_r} \quad \text{E19}$$

$$Z_r = \sqrt{L_r / C_r} \quad \text{E20}$$

3.4.4. quality element

The circuit's "goodness" or quality is gauged by the quality factor Q . This is the ratio of the power used by the resistance of the resonant circuit to the power dissipated in the reactance. Equation 21 or, alternatively, equation 22 can be used to define the quality factor Q .

$$Q = \omega_r \times L_r / R = 1/\omega_r \times C_r \times R = Z_r / R \quad \text{E21}$$

$$Q = 1/R \times \sqrt{L_r / C_r} \quad \text{E22}$$

3.4.5. Normalized amplitudes of the current and power in the series resonant circuit

The normalised amplitudes of the current and output power in the series resonant circuit are depicted in Figures 18 and 19, respectively, as functions of f_s/f_r and $R/Z_r = 1/Q$. When the load resistance is low and the resonance frequency is present, the

circuit's maximum current value occurs. It is also observed that at resonant frequency if the load $R \rightarrow 0\Omega$ then the peak current $I \rightarrow \infty$ and the system can be destroyed. According to this research, a short circuit on the load side is never likely. The output power is maximum at the resonance frequency and with minimal load resistance.

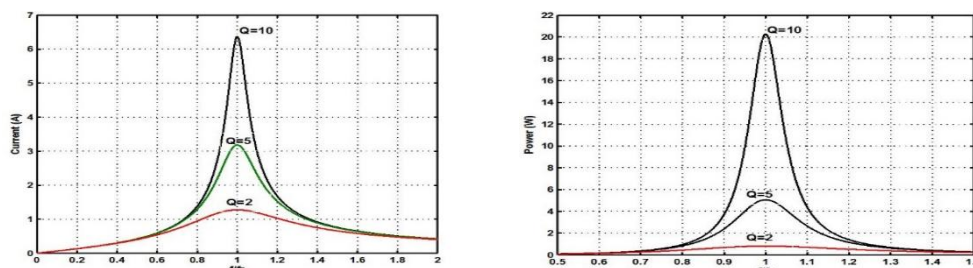


Figure 18. Amplitude of the current, Figure 19. Amplitude of the power

4. Control

The voltage loop, also known as the fast loop, and the PEM loop, also known as the slow loop, make up the control. The voltage controller is in charge of maintaining the converter's output voltage at a preset, constant value regardless of variations in load. The PEM controller is in charge of maintaining the PEM in its optimal state, This entails supplying the load with the necessary electrical power while using the least amount of current and, hence, hydrogen. The control scheme of the converter is illustrated in Figure 20.

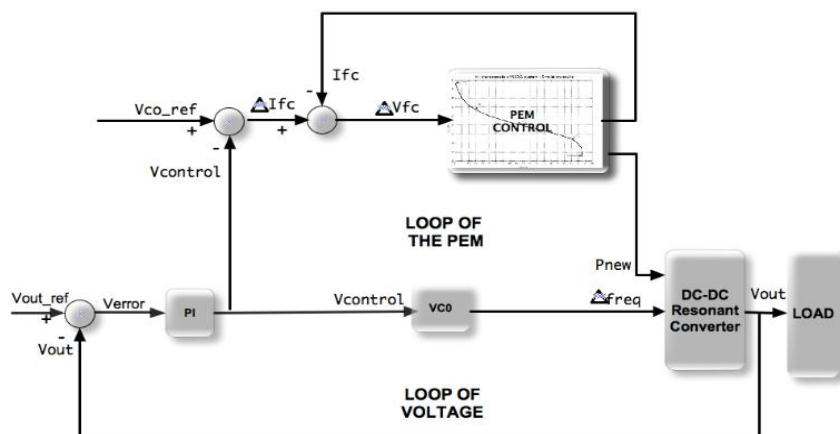


Figure 20: Control structure of the SRC

5. Experimental setup and results

The entire system, made up of the PEM Mark 1020, the SRC, and the load, is tested using it. The load is made up of a number of resistors connected in series, and a manual switch controls their variation. A typical dial pressure gauge measures the fuel pressure that powers a PEM stack and keeps it constant between 0.3 and 0.5bar. The oxidant flow required to

create the electrochemical reaction must be injected into the stack using the ventilator. The multimeter's representation of a voltage of 26.06V is the same as the PEM's open-circuit voltage. In order to experimentally confirm the SRC's stability and dynamics, This section reports the findings of the tests related to the output voltage and current, the PI controller, and the resonant current.

5.1. Fuel cell Output voltage and output current

The graph below demonstrates the stability of the converter's voltage control loop in that Notwithstanding changes in output current or the load, the output voltage, V_{out} , stays constant. Both circumstances fall under this requirement (Figure 21).

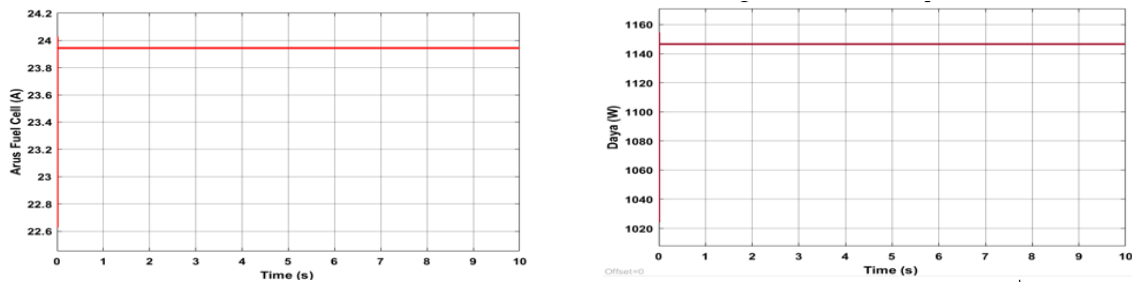


Figure 21. Output voltage (V_{out}) and output current (C_{out}).

Effects of hydrogen gas pressure characteristics on fuel cell voltage and current

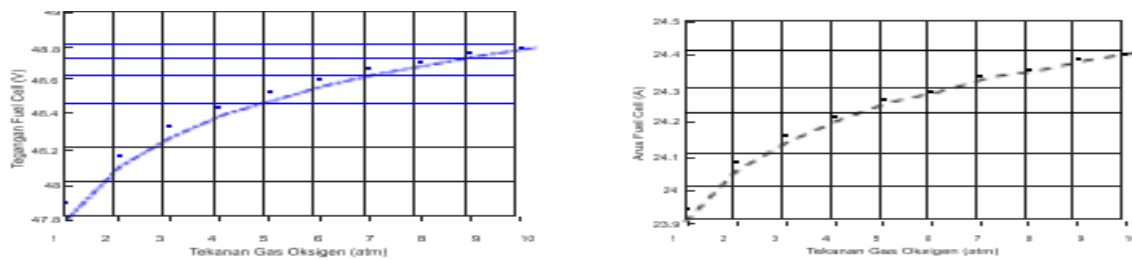


Figure 22. Hydrogen gas pressure on FC voltage and current

Temperature-related characteristics that affect the fuel cell's voltage and current.

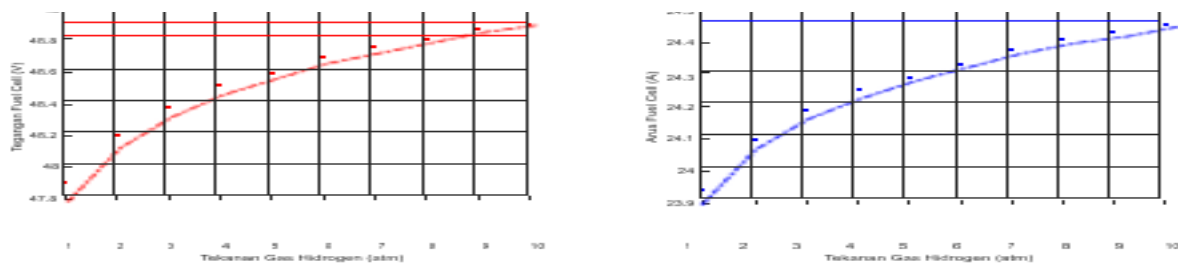


Figure 23. The voltage and current of the fuel cell fluctuate with temperature.

5.2. Proportional integral control (PI)

Analysis of the PI control signal can be used to gauge the dynamics of the system. Hence, after taking into account both load variation scenarios, it seems that the PI controller's stabilization time is around 7 ms. Also, it displays a minor oscillation that demonstrates how effectively the PI control's settings were chosen for the system. A step-up load situation is

represented by Situation 'a,' whereas a step-down load condition is represented by Situation 'b.' The voltage error is defined by INA101 as $=V_{\text{measured}} - V_{\text{reference}}$, and the objective of the PI controller is to lower this error for every change in load.

5.3. Resonant circuit operation

Adapts to both step-up and step-down load situations:

It follows from this research that the converter adjusts its operating frequency in response to changes in the load. As a result, the frequency is low for low load levels (I_{min} , R_{max}) and high for high load levels (I_{max} , R_{min}). We infer that the system has good dynamic characteristics since the change in frequency of operation is instantaneous in dynamic terms. It can also be seen that the output voltage V_{out} does not change regardless of the load variations. This research supports the controller's stated goal, which is to maintain a constant output voltage in order to meet the demands placed on power system applications.

7. Integrated system

A wind turbine, a hydrogen-fueled system, and a PV matrix make up the hybrid system under study. A solar system in a hydrogen fueled system consist of solar PV, DC/AC converter, PEM electrolyzer and water. We use fuel cells along with an off-grid hydrogen tank in hybrid energy systems (Figure 24). In similar way other type of hybrid PEMFC can be utilise.

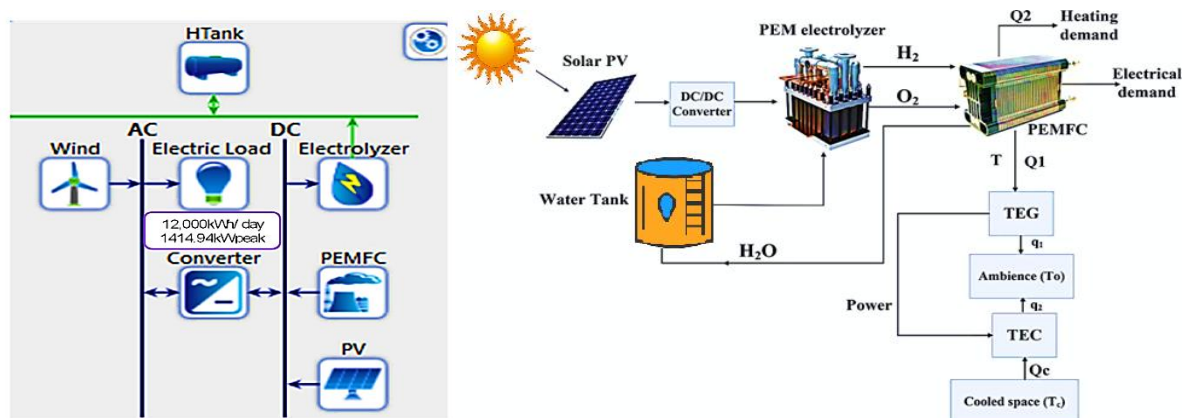


Figure 14 Hybrid system schematic diagram

8. Discussion

A noteworthy accomplishment was the operation of more than 25,000 fuel cell vehicles in 2020. The market for automotive fuel cells is anticipated to increase from 25,000 units in

2022 to 724,00 units in 2030, a CAGR of 52.4%. In the course of this research, fuel cell-powered buses, LCVs, lorries, and passenger automobiles were mapped. The development of long-distance fuel cell vehicles has been spurred by the rising demand for zero-emission commercial freight trucks and buses. The demand for FCEVs is anticipated to steadily rise as a result of the increasing global deployment of hydrogen infrastructure. Longer range and high-power engines are now possible in fuel cell electric vehicles thanks to technological advancements in fuel cell components and other fields (FCEVs). The demand for FCEVs will change as a result in the upcoming years. The further adoption of the technology is, however, slowed down by various constraints. The infrastructure for hydrogen is still lacking or not sufficiently developed. In addition, despite a general decline, FC costs are still costly, particularly because PEMFCs need a platinum-based catalyst to speed up reactions. In order to prevent the potential for irreversible voltage loss brought on by platinum contamination, At the anode side, PEMFC is required to employ a clean hydrogen stream. Due to these problems, the fuel cell lifespan is ultimately less than planned for traditional ICEs. Discussing the design and execution of a fuel cell-based power generation system is the main goal of the study. In light of this, a methodology for developing and putting into practise an effective high power converter system is described. The PEM fuel cell electrical equivalent model, which was tested using the commercial MARK 1020 system, is also included in the study. The series-resonant converter topology, whose foundation is based on soft-switching approach, is chosen after analysis of the converter topologies that are most appropriate for this application type and satisfying a number of criteria. The converter was created with low component stresses, high frequency operation, and soft-switching commutation in mind. It comprises of an input filter, a full-bridge inverter, a series resonant circuit, and a diode rectifier on the main side and an output filter on the secondary side. The operational limitations of the system MARK 1020 were taken into consideration when designing the converter.

9. Fuel Cell Systems Producers on the Market

Between 2017 and 2021, the overall shipment of units for all applications (transport, stationary, and portable) climbed by 22%, whilst the overall shipment of MWs increased by 251% within the same time frame. During the past few years, the fuel cell market has grown and it is anticipated to continue growing in order to meet 2030 goals. All fuel cell types shipped 658.6 MW in 2017; by 2021, this number has increased by a factor of 2.5 to 2313.1

MW [38]. Geographically, Asia, Europe, and North America make up the majority of the fuel cell market; in 2021, Asia had the highest share with 56.2 million units and 1493.2 MW of shipping power [38].

10. Conclusions

Special attention is provided to the controller, which keeps the converter's output voltage consistent, in order to fulfil the needs of the power system application and keep the PEM running within its ideal operating point. The voltage controller, and the control implementation were divided into two which is in charge of maintaining the converter's output voltage constant despite variations in loading, and the PEM controller, which is in charge of enhancing performance by maintaining the PEM fuel cell at its optimum operating point. Due to the significance of the PEM cell behaviour, the findings are first provided for the PEM fuel cell model and then for the overall system under load. The results demonstrate that the converter used is a solid choice to support the approach for boosting PEM fuel cell efficiency because it enables appropriate control of the power delivered by the fuel cell and complies with load regulation requirements while incurring the fewest losses possible thanks to the use of soft switching commutation.

REFERENCES

1. Corrêa, J.M., et al. An electrochemical-based fuel cell model suitable for electrical engineering automation approach. *IEEE Transactions on Industrial Electronics*, 2004; 5(51) 1103-1112.
2. Yu, D. and S. Yuvarajan. A novel circuit model for pem fuel cells. *Proceedings of IEEE Applied Power Electronics Conference and Exposition*. 2004.
3. Friede, W., S. Raël, and B. Davat. Mathematical model and characterization of the transient behavior of a PEM fuel cell. *IEEE Transactions on Power Electronics* 2004; 5(19) 1234-1241.
4. Forrai, H., Yanagita Y., and Kato Y. Fuel-cell parameter estimation and diagnostics. *IEEE Transactions on Energy Conversion*, 2005; 3(20): 668-675.
5. Outeiro, M.T., et al., A Parameter Optimized Model of a PEM Fuel Cell Including Temperature Effects. *Journal of Power Sources*, 2008; 185(2) 952-960.
6. Outeiro, M.T., et al. Dynamic Modeling and Simulation of an Optimized Proton Exchange Membrane Fuel Cell System. *Proceedings of International Mechanical Engineering Congress and Exposition*. Seattle, USA. ASME; 2007.
7. Kristina Haraldsson, K.W. Evaluating PEM fuel cell system models. *Journal of Power Sources*, 2004; 126(1-2) 88-97.

8. Bernardi, D.M. and Verbrugge M.W. A mathematical model of the solid-polymer-electrolyte fuel cell. *Journal of Electrochemical Society*, 1992; 2477–2491.
9. Rowe, A. and Li X. Mathematical modelling of proton exchange membrane fuel cells. *Journal of Power Sources*, 2001; 82-96.
10. Mann, R.F., et al. Development and application of a generalised steady-state electrochemical model for a PEM fuel cell. *Journal of Power Sources*, 2000; 173-180.
11. Amphlett, J.C., et al. A model predicting transient responses of proton exchange membrane fuel cells. *Journal of Power Sources*, 1996; 183-188.
12. Wang, C. and Nehrir M. Dynamic models and model validation for PEM fuel cells using electrical circuits. *IEEE Transactions on Energy Conversion*, 2005; 2(20) 442-451.
13. Andersen, G.K., et al. A new power converter for fuel cells with high system efficiency. *International Journal of Electronics*, 2003; 90(11-12) 737-750.
14. Xu, H., Kong L., and Wen X. Fuel Cell Power System and High Power DC–DC converter. *IEEE Transactions on Power Electronics*, 2004; 19(5) 1250-1255.
15. Shiju, W. Design and hardware implementation of a soft-switched converter for fuel cell applications. MSc thesis. University of Texas; 2006
16. Krykunov, O. Comparison of the DC/DC-Converters for Fuel Cell Applications. *International Journal of Electrical Computer and Systems Engineering*, 2007; 1(1) 71-79.
17. Rathore, A., Bhat A., and Oruganti R. A Comparison of Soft-Switched DC-DC Converters for Fuel Cell to Utility Interface Application. *IEEE Proceedings*, 2007; 588-594.
18. Rong-Jong, W. and Rou-Yong D. High-Efficiency Bidirectional Converter for Power Sources With Great Voltage Diversity. *IEEE Transactions on Power Electronics*, 2007; 22(5) 1986-1996.
19. Ying-Chun Chuang, Y.-L.K., Hung-Shiang Chuang, Hung-Kun Chen Implementation and Analysis of an Improved Series-Loaded Resonant DC–DC Converter Operating Above Resonance for Battery Chargers. *IEEE Transactions on Industry Applications*, 2009; 45(3) 1052 – 1059.
20. Cancelliere P., et al. Modeling and Control of a Zero-Current-Switching DC/AC Current-Source Inverter. *IEEE Transactions on Industrial Electronics*, 2007; 54(4) 2106-2119.
21. Lee Y.-S., Chiu Y.-Y. and Cheng M.-W. Inverting ZCS Switched-Capacitor Bi-directional Converter, 37th IEEE Power Electronics Specialists Conference, Jeju, Korea, PESC; 2006.
22. Yuang-Shung, L., et al. Multiple Output Zero-Current Switching Bi-directional Converter. 33rd Annual Conference of the IEEE Industrial Electronics Society, Taiwan Japan, IECON; 2007.
23. Mohan N. and Underland T. *Power Electronics Converters Applications and Design*. John Wiley and Sons, Inc. 2003.
24. Peng, F.Z., et al. A New ZVS Bidirectional DC–DC Converter for Fuel Cell and Battery Application. *IEEE Transactions on Power Electronics*, 2004; 19(1) 54-65.
25. Krykunov O. Comparison of the DC/DC-Converters for Fuel Cell Applications. *International Journal of Electrical Computer and Systems Engineering*, 2007; 1(1) 71-79.
26. Lee J.-Y., Jeong Y.-S. and Han B.-M. An Isolated DC/DC Converter Using High-Frequency Unregulated LLC Resonant Converter for Fuel Cell Applications. *IEEE Transactions on Industrial Electronics*, 2011; 58(7) 2926 - 2934.

27. Xin Kong, A.M.K., Analysis and Implementation of a High Efficiency Interleaved Current-Fed Full Bridge Converter for Fuel Cell System. *IEEE Transactions on Power Electronics*, 2007; 22(2) 543-550.
28. Averberg A., Meyer K.R. and Mertens A. Current-fed full bridge converter for fuel cell systems. *IEEE Power Electronics Specialists Conference, Rhodes, Greece. PESC; 2008.*
29. Changchien S., Liang T., Chen J. and Yang L. Novel High Step-Up DC–DC Converter for Fuel Cell Energy Conversion System. *IEEE Transactions on Industrial Electronics*, 2010; 57(6) 2007 – 2017.
30. Blaabjerg F., Chen Z. and Kjaer S.B. Power Electronics as Efficient Interface in Dispersed Power Generation Systems. *IEEE Transactions on Power Electronics*, 2004; 19(5) 1184-1194.
31. Outeiro M. T. and Carvalho A., “Methodology of Designing Power Converters for Fuel Cell Based Systems: A Resonant Approach,” *New Developments in Renewable Energy*, Mar. 2013,
32. Elkafas AG, Rivarolo M, Gadducci E, Magistri L, Massardo AF. Fuel Cell Systems for Maritime: A Review of Research Development, Commercial Products, Applications, and Perspectives. *Processes*, 2023; 11(1):97.
33. Girirajan, B.; Shekhar, H.; Lai, W.-C.; Jagannathan, H.K.; Bidare Divakarachar, P. High Gain Converter with Improved Radial Basis Function Network for Fuel Cell Integrated Electric Vehicles. *World Electr. Veh. J.* 2022,13, 31.
34. Raghavendra KVG, Zeb K, Muthusamy A, Krishna TNV, Kumar SVSVP, Kim D-H, Kim M-S, Cho H-G, Kim H-J. A Comprehensive Review of DC–DC Converter Topologies and Modulation Strategies with Recent Advances in Solar Photovoltaic Systems. *Electronics*. 2020; 9(1):31
35. K.H. Liu and F. C. Lee, Zero-voltage switching technique in DC/DC converters, *IEEE Trans. Power Electron*, 1990, vol. 5, no. 3, pp. 293–304,.
36. W. A. Tabisz and F. C., “Zero-voltage- switching multi-resonant technique—A novel approach to improve performance of high frequency quasi-resonant converters”, in *Proc. Power Electron. Spec. Conf.*, 1988, vol. 1, no. 11–14, pp. 9–17.
37. Mubarak H. and Santoso T.H.,” Monitoring of Hydrogen Fuel Cell Modeling with Boost Converter”, *J. Phys.: Conf. Ser.* 1844 , 2021, 012018
38. Renewables. Global Status Report. REN21 (Renewable Energy Policy Network for the 21st Century). Available online: <http://www.ren21.net/status-of-renewables/global-statusreport/> (accessed on 11 November 2020).
39. Bonsrulah Al., Hussein A.Z., Mohammed J. Alshukri, Lama M. Mikhaeel, Noor N. AL-sawaf, Kefif Nesrine, M.V. Reddy, and Karim Zaghbi, "Design and Simulation Studies of Hybrid Power Systems Based on Photovoltaic, Wind, Electrolyser, and PEM Fuel Cells" 2021, *Energies* 14, no. 9: 2643.
40. Marefati, M., Mehrpooya M., Introducing a hybrid photovoltaic solar, proton exchange membrane fuel cell and thermoelectric device system, *Sustainable Energy Technologies, and Assessments*, 2019, Volume 36, 100550, ISSN 2213-1388,